One-step fabrication of P_2O_5-loaded-TiO_2 composite with trace amounts of rGO as thin films for enhanced photovoltaic and photocatalytic performance

A. M. FLOREA[1,2,*], A. M. IORDACHE[1,*], S. CARAMIZOIU[1]
[1]*National Institute of Research and Development for Optoelectronics-INOE 2000, 077125 Magurele, Romania*
[2]*Faculty of Physics, University of Bucharest, 077125 Magurele, Ilfov, Romania*

In this work, a one-step sol gel method is reported for the fabrication of P_2O_5-loaded-TiO_2 composite with trace amounts of rGO as thin films (TiO_2+rGO+P_2O_5) with enhanced photocatalytic and photovoltaic performance. The sols containing titanium and phosphorus precursors with 0.2-0.7 wt% reduced graphene oxide (rGO) were spin-coated onto glass substrates in three and five layers, followed by thermal treatment at 400-500°C. FTIR, UV-Vis, and SEM analyses confirmed uniform morphology and adequate interfaces. The synergistic incorporation of P_2O_5 and rGO improved charge transport by promoting efficient charge separation and suppressing electron-hole recombination, while extending light absorption into the visible region. The performance of the films was strongly influenced by the rGO content, film thickness, and annealing temperature. These nanocomposite films offer a simple, cost-effective, and scalable approach for applications in photovoltaic devices, where they can function as efficient electron transport layers or photoanodes, as well as in photocatalytic environmental remediation.

(Received April 20, 2026; accepted June 2, 2026)

Keywords: TiO_2, P_2O_5, Thin film synthesis, Reduced graphene oxide, Optoelectronic properties

1. Introduction

Thin film oxide-semiconductors have attracted significant attention in recent years due to their wide range of applications in photocatalysis, chemical sensing, optoelectronics, and energy conversion devices. Among these materials, titanium dioxide (TiO_2) is one of the most extensively studied semiconductor oxides, owing to its high chemical stability, non-toxicity, relatively low cost, and favourable optical properties. These characteristics make it particularly suitable for applications such as the photocatalytic degradation of pollutants, self-cleaning surfaces, photoelectrochemical systems, and functional layers in energy-related technologies [1-5]. However, the performance of TiO_2 based materials is often limited by the rapid recombination of photogenerated electron-hole pairs and by their predominant absorption in the ultraviolet region of the electromagnetic spectrum [6-8]. To overcome these limitations, numerous recent studies have explored modifying the structure and composition of TiO_2 based materials through doping or by forming composites with other functional materials. The integration of two-dimensional carbon materials, particularly reduced graphene oxide (rGO), has been extensively investigated due to its high electrical conductivity, large specific surface area, and the ability of rGO to facilitate charge carrier transport and separation [9,10]. The interfacial interaction between TiO_2 and graphene can lead to reduced electron-hole recombination and enhanced photocatalytic or photoelectrochemical performance of the composite materials. Furthermore, TiO_2 carbon hybrid structures can exhibit improved optical and electronic properties due to efficient charge transfer between the constituent phases.

In addition to incorporating carbonic materials, introducing secondary oxides into the TiO_2 matrix is an effective strategy to tailor structural and surface properties. Phosphorus oxides, such as P_2O_5, can modify the oxide network, surface acidity, and adsorption behaviour of reactant molecules. Combining TiO_2 with P_2O_5 and conductive carbon materials can thus yield multifunctional composites with enhanced catalytic and optoelectronic performance [11-13].

TiO_2 based thin films and their composites are commonly fabricated *via* physical or chemical vapor deposition, sputtering, or plasma-assisted techniques [14-18]. While these methods allow precise control over film structure and composition, they typically require expensive equipment and stringent conditions, including high vacuum or elevated temperatures. Recently, solution-based deposition methods have gained attention due to their simplicity and lower cost. Among them, spin-coating is widely used to produce uniform thin films on various substrates [19, 20].

Spin-coating enables relatively precise control of film thickness and uniformity by adjusting parameters such as rotation speed, deposition time, and precursor solution properties [21, 22]. Recent studies have shown that rotation speed significantly affects the morphology, optical, and structural properties of metal oxide thin films [23]. For instance, TiO_2-ZnO composites prepared *via* sol-gel and spin-coating exhibit improved structural and optical

characteristics through careful optimization of deposition parameters. Similarly, TiO_2 thin films fabricated by sol-gel spin-coating demonstrate favourable optical and structural properties for photovoltaic and photocatalytic applications [24-26]. Porous TiO_2 films and doped variants have further shown enhanced photocatalytic activity [13, 27].

Another function for TiO_2 graphene composites that has attracted significant attention is due to their enhanced charge transport properties and improved photocatalytic efficiency. The incorporation of graphene facilitates effective charge separation and suppresses electron-hole recombination by acting as an electron acceptor and conductive pathway, resulting in superior photocatalytic and electrochemical performance, as well as improved optical absorption and surface characteristics [28, 29].

In particular, TiO_2 graphene thin film architectures have demonstrated strong potential in photovoltaic (PV) applications, where efficient charge transport and minimized recombination losses are essential. Recent studies on TiO_2/rGO based photoanodes and thin films report enhanced electron mobility, prolonged carrier lifetime, and significantly improved power conversion efficiency due to the synergistic interaction between TiO_2 and graphene components [30].

In this context, the development of simple, scalable, and cost-effective deposition techniques for TiO_2 based composite thin films remains highly desirable for device integration [31]. In this work, we propose a one-step spin-coating approach for the fabrication of P_2O_5-loaded-TiO_2 composite with trace amounts of rGO (abbreviated as TiO_2+rGO+P_2O_5) thin films directly onto glass substrates using a single precursor solution containing titanium and phosphorus compounds together with small amounts of reduced graphene oxide. This strategy enables the formation of functional composite films without the need for complex equipment or vacuum-based processes, offering a facile and scalable route for thin-film fabrication. Compared to other methods, such as magnetron sputtering [32, 33] or spray pyrolysis deposition [34], our approach has the advantage of delivering a stable solution that can be stored and used at a later date, for up to three months.

2. Experimental procedure

Thin composite layers were deposited on optical glass substrates (Thorlabs, Newton, New Jersey, United States) using spin coating (Laurell 650, Laurell Technologies Corporation, Lansdale, USA) at 2000 rpm for 1 minute. The synthesis conditions for the films are summarized in Table 1. The TiO_2 solution doped with rGO and P_2O_5 was prepared by dissolving 1.8 mL of titanium isopropoxide (Merck KGaA, Darmstadt, Germany) in 18 mL of isopropyl alcohol (Merck KGaA, Darmstadt, Germany), followed by the addition of 2 mL of 37% HCl (Chimopar, Romania) to prevent precipitation. The resulting transparent yellow solution was then doped with the required volume of rGO dispersion, prepared by dispersing rGO powder (Abalonix, Porsgrunn, Norway) in distilled water at a concentration of 1 mg/mL, together with 0.083 mL of H_3PO_4 (Merck KGaA, Darmstadt, Germany), and mechanically stirred for 72 hours before deposition. Deposition was performed by dropping 20 droplets of the solution onto the slide, followed by spin coating for 1 minute. Between layers, the slides were heated on a hot plate at 80°C. For three-layer samples, green iridescence was observed, while five-layer samples showed initial pink iridescence that turned pale green after heating (see Fig. 1).

Thermal treatment included drying at 200°C (heating rate 50°C/h, 30-minute dwell) and calcination at 400, 450, and 500°C (heating rate 50°C/h, 30-minute dwell) in an industrial oven (Caloris, Romania). Cooling was performed freely at room temperature.

Table 1. Synthesis conditions for TiO_2+rGO+P_2O_5 samples

Sample name	Ti isopropoxide (mL)	Isopropyl alcohol (mL)	H_3PO_4 (mL)	rGO (mg)	HCl (mL)	Temperature (°C)	No. of layers
$TiO_2P_2O_5$rGO 0.2%	1.8	18	0.083	0.972	2	400, 450, 500	1, 3, 5
$TiO_2P_2O_5$rGO 0.5%	1.8	18	0.083	2.43	2	400, 450, 500	1, 3, 5
$TiO_2P_2O_5$rGO 0.7%	1.8	18	0.083	3.402	2	400, 450, 500	1, 3, 5

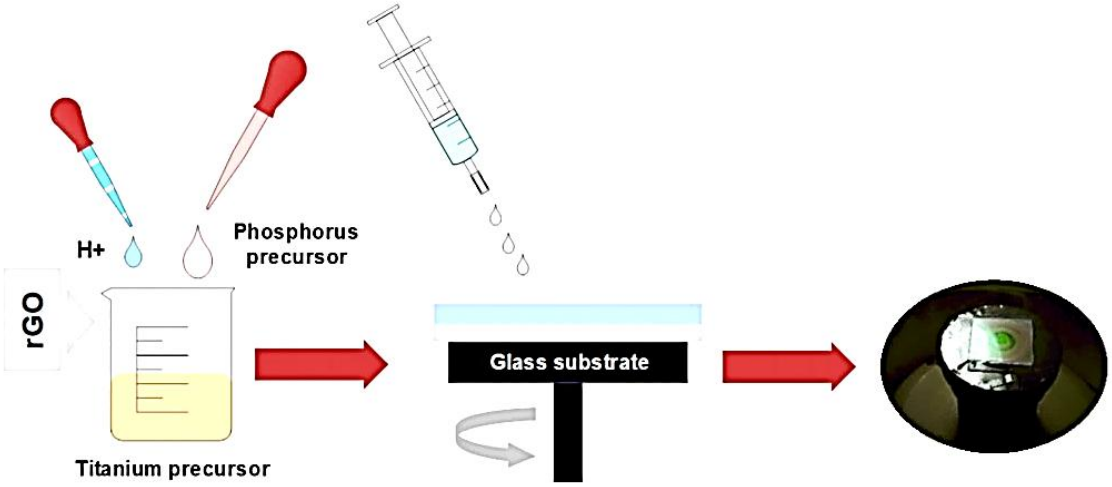

Fig. 1. Layer-by-layer fabrication of TiO_2+rGO+P_2O_5 thin films: from sol preparation to spin-coated deposition (colour online)

Fourier-transform infrared (FTIR) spectra were recorded using a Perkin Elmer Spectrophotometer-Spectrum 100 provided with the Universal Attenuated Total Reflectance (UATR) accessory, in the range of 380–4000 cm^{-1}, with 1 cm^{-1} resolution, 20 total scans and a measurement error of ±0.1%. The optical properties were measured with a Spectrophotometer Lambda 1050 (PerkinElmer, Waltham, MA, USA) in the UV-Vis-NIR domain in the range of 300-1800 nm, with a measurement error of ±0.03%. The morphology and elemental composition of the samples were investigated using scanning electron microscopy (SEM) coupled with energy-dispersive X-ray (EDX) analysis, performed on an FEI Inspect F50 system (FEI Europe B.V., Eindhoven, The Netherlands).

3. Results and discussions

The FT-IR spectra of the TiO_2+rGO+P_2O_5 nanocomposite thin films reveal a clear structural evolution depending on the thermal treatment temperature and dopant concentration. In all analysed samples, the spectral region between 500-900 cm^{-1} exhibits absorption bands associated with Ti-O and Ti-O-Ti vibrational modes, confirming the formation of the titanium dioxide network [25]. The main signature of phosphorus doping is represented by the intense and broad band centred around 1030-1050 cm^{-1}, which is attributed to the stretching vibrations of phosphate groups (P–O and P=O) as well as Q^n-type structural units [35]. The intensity of these bands increases significantly for samples with five deposited layers, suggesting the formation of an optimal density of active sites that can facilitate dye adsorption in dye-sensitized solar cells. The presence of the rGO phase is confirmed by the band located at approximately 1610 cm^{-1}, corresponding to C=C vibrational modes of the graphitic structure [36]. The improved definition of this peak at 500°C indicates a high thermal stability of the carbon support and a higher degree of graphene oxide reduction.

Furthermore, the broad band around 3400 cm^{-1}, associated with hydroxyl groups (-OH), shows very low intensity in all spectra, suggesting that the calcination process led to an effectively dehydroxylated surface [37]. This feature is important because it reduces the density of charge-carrier recombination centres. In addition, the relatively sharp band observed at approximately 2350 cm^{-1} at 400°C, attributed to adsorbed CO_2 molecules or residual organic species from the precursors, significantly decreases in intensity at 500°C [38]. This behaviour indicates the formation of purer and more crystalline films at higher treatment temperatures, a factor that is essential for improving photoelectrochemical performance and enhancing photocurrent generation in photovoltaic devices. The FT-IR spectra of the TiO_2+rGO+P_2O_5 nanocomposite thin films are shown in Fig. 2, illustrating the structural evolution with increasing thermal treatment temperature and dopant concentration.

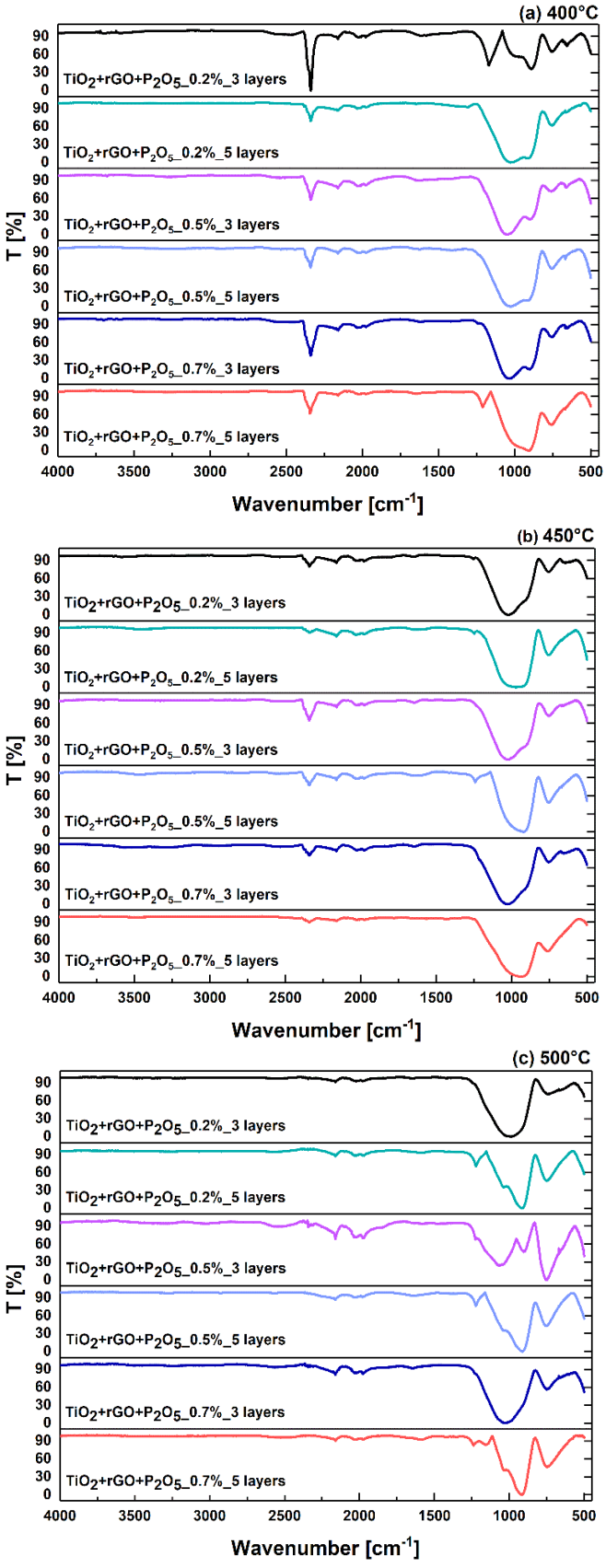

Fig. 2. FT-IR spectra of TiO_2+rGO+P_2O_5 nanocomposite thin films deposited with different numbers of layers and thermally treated at a) 400°C, b) 450°C and c) 500°C (colour online)

The analysis of the optical transmission spectra (Fig 3. a–c) reveals a strong dependence of the dielectric properties of the TiO_2+rGO+P_2O_5 composite thin films on both the deposition parameters and the annealing temperature. All samples exhibit well-defined interference fringes across the visible (400-800 nm) and near-infrared (800-1800 nm) regions, confirming the formation of high-quality, homogeneous thin films. It is observed that increasing the number of layers from 3 to 5 induces a redshift in the interference maxima, a phenomenon attributed to the increase in physical film thickness, while the peak transmittance decreases slightly due to enhanced absorption and scattering at additional interfaces. The effect of thermal treatment is evidenced by the more pronounced interference patterns at 500°C compared to 400°C, suggesting improved crystallinity of the TiO_2 phase and a potential densification of the P_2O_5 glass matrix. Furthermore, the presence of reduced graphene oxide (rGO) modulates the overall transmittance to values below 60−65%, playing a critical role in tuning the complex refractive index of the system, as can be seen from Fig. 3. These results demonstrate that through precise control of the dopant concentration and thermal regime, thin films with tailored optical properties can be engineered for applications in photocatalysis or optical sensors.

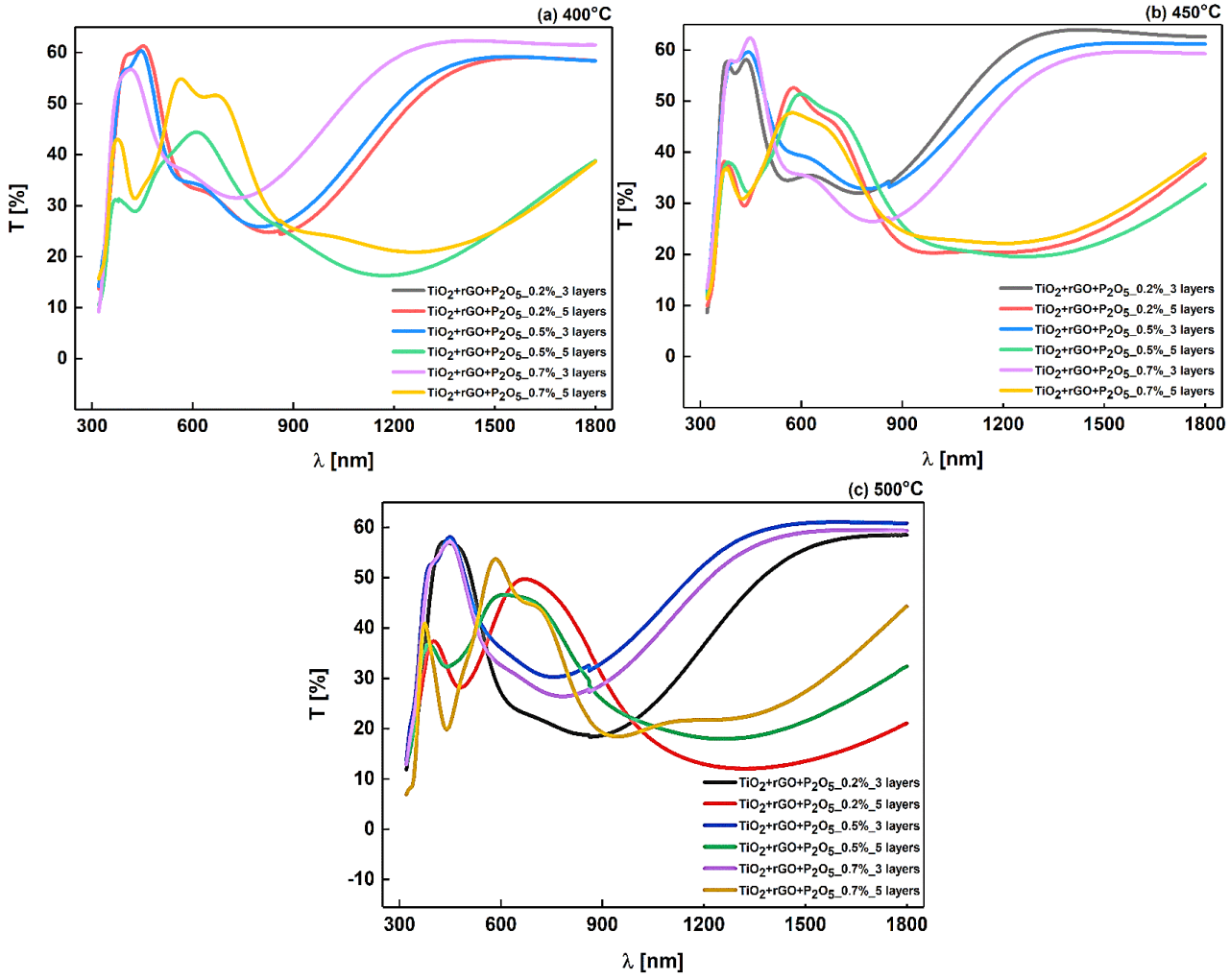

Fig. 3. Optical transmittance spectra of TiO_2+rGO+P_2O_5 composite thin films as a function of wavelength (λ) for samples annealed at: (a) 400°C, (b) 450°C, and (c) 500°C, illustrating the effects of P_2O_5 concentration (0.2%, 0.5%, 0.7%) and the number of deposition layers (3 and 5 layers) (colour online)

The optical absorbance spectra (Fig. 4 a-c) further clarify the influence of structural parameters on light–matter interactions within the TiO_2+rGO+P_2O_5 composite system. In addition to the fundamental UV absorption edge, the spectra are characterized by pronounced interference-related maxima, whose positions shift systematically with increasing film thickness and P_2O_5 content. A notable increase in absorbance in the near-infrared (NIR) region is observed for films annealed at 500°C. This behaviour likely reflects a synergistic effect between the improved crystallinity and densification of the TiO_2 anatase phase and the thermally induced restoration of the π-electron network in reduced graphene oxide (rGO), which enhances electronic delocalization and optical absorption in the composite matrix. Fig. 4 shows that the peaks in the 400-1400 nm region correspond to constructive interference maxima, while the sharp increase below 350 nm represents the fundamental absorption edge of the TiO_2 matrix [39].

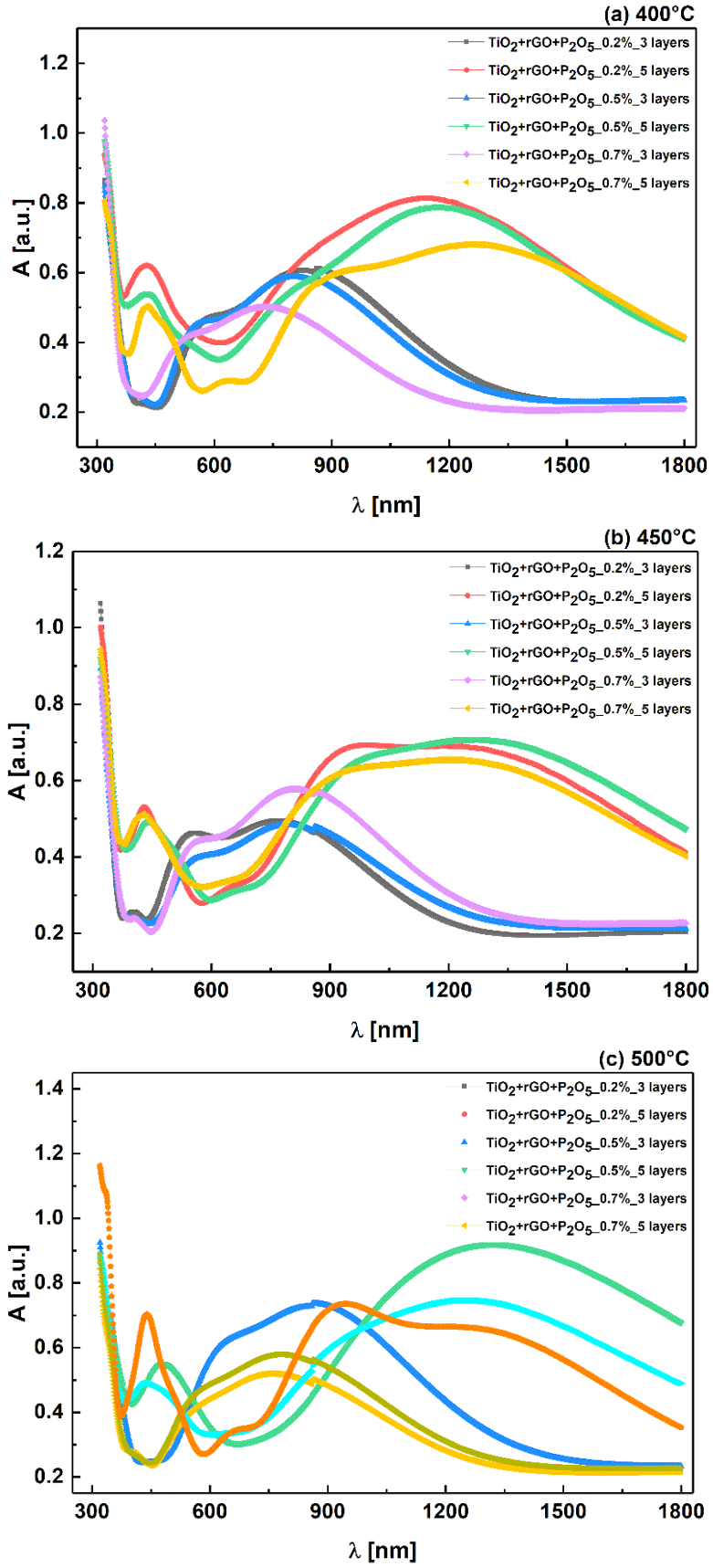

Fig. 4. Wavelength-dependent absorbance spectra of TiO_2+rGO+P_2O_5 multi-layered films under varying annealing conditions (400–500°C) (colour online)

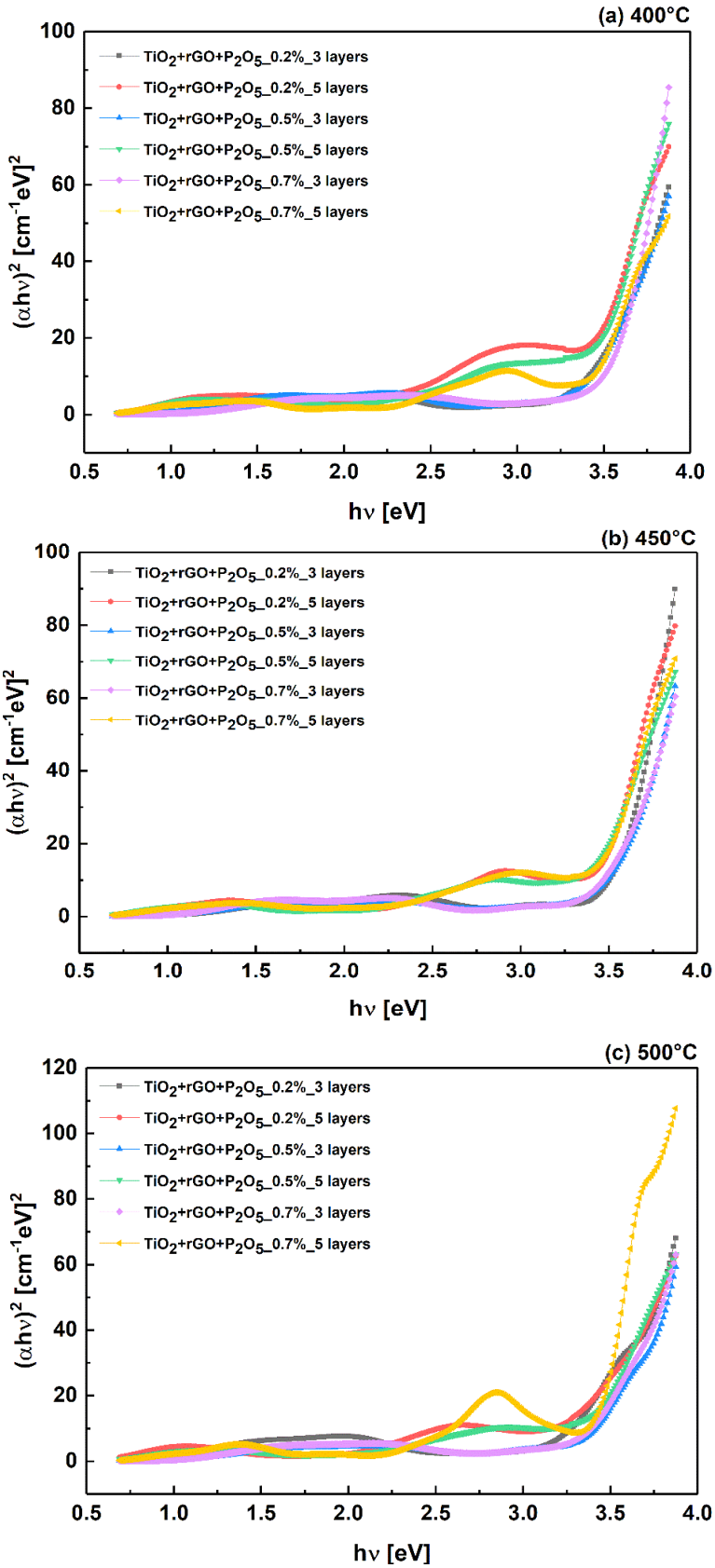

Fig. 5. Tauc plots of $(\alpha h\nu)^2$ versus photon energy ($h\nu$) for TiO_2+rGO+P_2O_5 composite thin films annealed at: a) 400°C, b) 450°C, and c) 500°C (colour online)

The optical band gap (E_g) of the TiO_2+rGO+P_2O_5 thin films was determined by extrapolating the linear portion of the $(\alpha h\nu)^2$ versus $h\nu$ curves to the energy axis, according to the Tauc relation for direct transitions, where B is the Tauc

parameter: $(\alpha h\nu)^2=B^2(h\nu-E_g)$ [40]. The thermal evolution of the electronic structure was systematically evaluated by comparing the Tauc plots across the three annealing temperatures (Fig. 5 a-c). As summarized in Table 2, a consistent narrowing of the optical bandgap is observed as the temperature increases from 400°C to 500°C. This trend is primarily attributed to the thermal densification of the TiO_2 matrix and the transition toward a more ordered crystalline anatase phase, which reduces the density of amorphous-related defects and facilitates electronic transitions. The data highlights a significant synergistic effect between the number of deposition layers and the dopant concentration. The 5-layer configuration consistently yields lower E_g values compared to the 3-layer counterparts, suggesting that increased film thickness promotes a more effective percolation of rGO within the oxide host. Notably, the sample containing 0.5% P_2O_5 with 5 layers achieved the lowest bandgap of 3.21 eV at 500°C. This indicates an optimal doping threshold where phosphorus atoms and reduced graphene oxide clusters work in tandem to create mid-gap states, as evidenced by the absorption tails in the visible region. Conversely, the blueshift observed for the 0.7% P_2O_5 samples suggests that excessive phosphorus may lead to structural strain or a Burstein-Moss-like shift, effectively widening the gap [41].

Table 2. Dependence of the optical energy gap on the dopant stoichiometry and thermal treatment parameters for multi-layered TiO_2 composites

Sample ID	rGO (%)	No. of layers	E_g at 400°C (eV)	E_g at 450°C (eV)	E_g at 500°C (eV)
S1	0.2	3	3.45	3.40	3.36
S2	0.2	5	3.38	3.31	3.25
S3	0.5	3	3.42	3.35	3.30
S4	0.5	5	3.32	3.28	3.21
S5	0.7	3	3.60	3.52	3.48
S6	0.7	5	3.50	3.44	3.41

A synergistic interfacial charge transfer mechanism is responsible for the improved optoelectronic and photocatalytic performance of the TiO_2+rGO+P_2O_5 composite films. Because of its high electrical conductivity and advantageous work function, which serves as an electron acceptor and transport channel, the photogenerated electrons in the TiO_2 conduction band are effectively transferred to the rGO phase. By spatially segregating charge carriers, this method dramatically reduces electron-hole recombination. By adding phosphate-related defect states and increasing surface acidity, the addition of P_2O_5 to the TiO_2 matrix simultaneously alters the local electronic structure, encouraging reactant species adsorption and facilitating interfacial charge transfer processes. The formation of shallow trap states contributes to band gap narrowing and extended visible-light absorption at optimal concentrations (0.5% P_2O_5). However, structural distortion and potential carrier scattering are induced by an excessive phosphorus content (0.7%), resulting in reduced efficiency. This is why, the functional performance of the composite films is ultimately enhanced by the combined effects of enhanced carrier mobility and protracted charge carrier lifetime, which are the result of the formation of conductive percolation pathways through rGO and the improved crystallinity at higher annealing temperatures. Our results are in line with the results obtained for other similar materials, which are summarized in Table 3.

Table 3. Comparison of the results with other compounds

Compound	Additive content	Temp (°C)	E_g (eV)	Ref.
S4	0.5% rGO	500	3.21	Our study
Al_2O_3-TiO_2	49.5%	700	3.4	[4]
TiO_2	Double layer	500	3.242	[13]
Nb-TiO_2	10% Nb	600	3.64	[25]

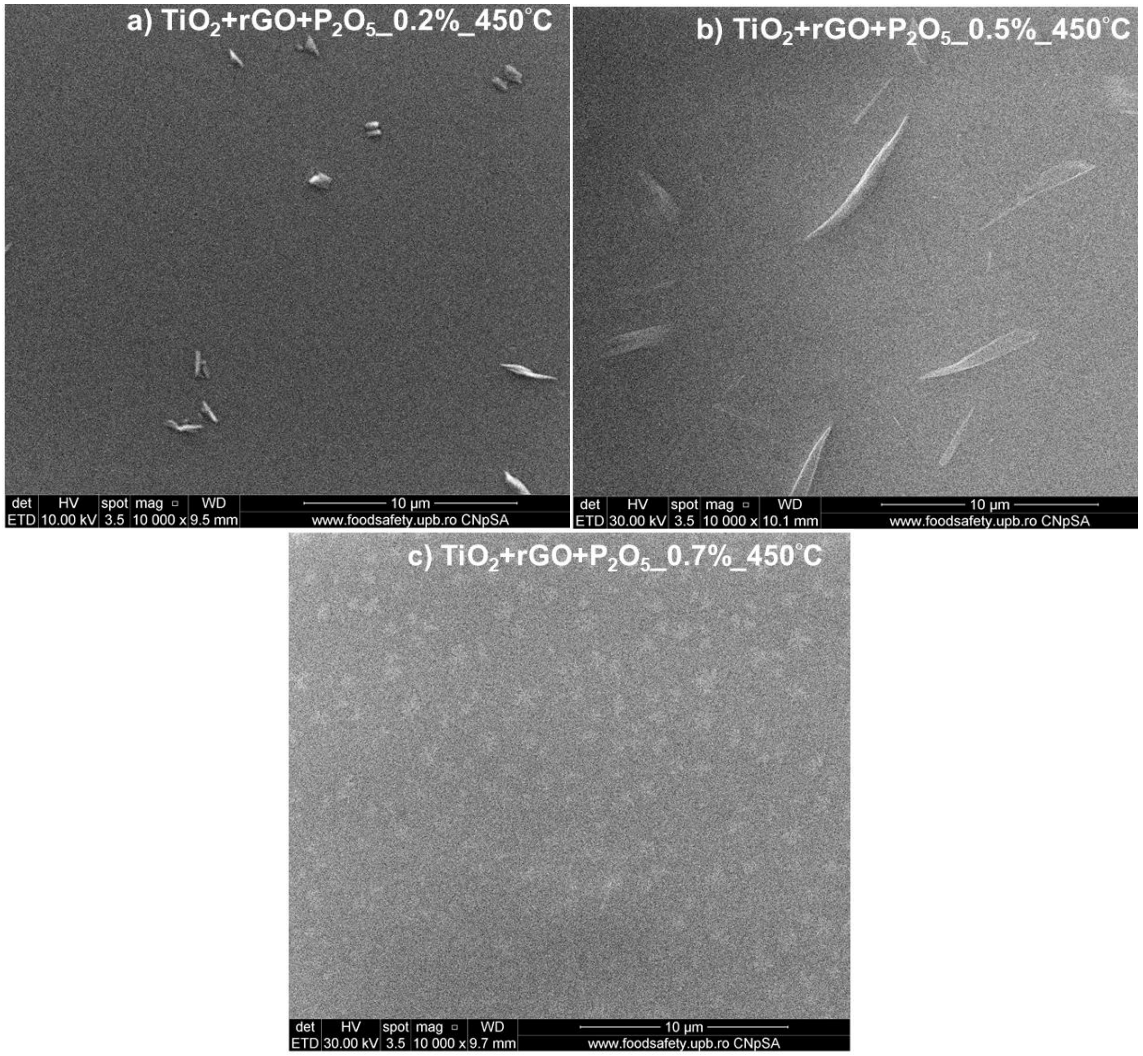

Fig. 6. SEM micrographs of TiO_2/P_2O_5 composites calcined at 450°C with varying P_2O_5 content

The SEM micrographs of the TiO_2+rGO+P_2O_5 composites calcined at 450°C from Fig. 6 show that the rGO concentration stays constant while the P_2O_5 content controls the observed morphological changes. With comparatively large TiO_2+P_2O_5 particles and a dense, aggregated structure, the TiO_2+rGO+P_2O_5 0.2% sample suggests little control over particle growth at low P_2O_5 loading. A more refined morphology with smaller, more evenly dispersed particles and better surface uniformity results from raising the P_2O_5 level to 0.5%. Although some degree of particle clustering is still visible, the structure of the TiO_2+rGO+P_2O_5 0.7% sample becomes more open and porous, suggesting that a greater P_2O_5 content encourages the development of a more linked framework.

4. Conclusions

In this work, TiO_2+rGO+P_2O_5 nanocomposite thin films were successfully fabricated using a one-step sol-gel spin-coating approach, demonstrating a simple, cost-effective, and scalable route for multifunctional oxide coatings. Structural and spectroscopic analyses confirmed the formation of homogeneous, well-integrated composite films, with improved crystallinity and reduced defect density at higher annealing temperatures. The incorporation of reduced graphene oxide and phosphorus oxide leads to a pronounced synergistic effect, enhancing charge separation efficiency, suppressing electron-hole recombination, and extending optical absorption into the visible and near-infrared regions. A systematic dependence of the optical properties on dopant concentration, number of layers, and thermal treatment was observed. The optical band gap decreases with increasing annealing temperature and film thickness, reaching a minimum value of 3.21 eV for the optimized composition (0.5% P_2O_5, 5 layers, 500°C), indicating effective electronic coupling and improved charge transport pathways within the composite structure. The results also highlight the existence of an optimal doping threshold, beyond which structural disorder and band-filling effects may counteract performance gains.

Overall, the developed TiO_2+rGO+P_2O_5 thin films exhibit tunable structural and optical properties, making them promising candidates for applications in photovoltaic devices as electron transport layers or photoanodes, as well as in photocatalytic systems for environmental remediation.

The proposed fabrication strategy and compositional optimization provide valuable insights for the design of next-generation hybrid oxide materials with enhanced functional performance.

Acknowledgements

The authors were supported by the Core Program with the National Research Development and Innovation Plan 2022-2027, carried out with the support of Ministry of Education and Research, project no. PN 23 05.

References

[1] P. Szołdra, M. Frąc, A. Adamczyk, M. Kot, W. Pichór, Materials Science and Engineering B **301**, 117189 (2024).
[2] Y. Xiong, S. Ma, X. Hong, J. Long, G. Wang, Molecules **28**, 7967 (2023).
[3] S. Tian, Y. Feng, Z. Zheng, Z. He, Coatings **13**, 1472 (2023).
[4] M. A. Camacho-González, I. V. Lijanova, J. Reyes-Miranda, E. Sarmiento-Bustos, M. Quezada-Cruz, P. Vera-Serna, M. Á. Barrón-Meza, A. Garrido-Hernández, Catalysts **13**, 1351 (2023).
[5] I. Chilibon, I. C. Vasiliu, J. Optoelectron. Adv. M. **27**(9-10), 511 (2025).
[6] X. Liang, S. Yu, B. Meng, X. Wang, C. Yang, C. Shi, J. Ding, Catalysts **15**, 542 (2025).
[7] A. J. Jadhav, A. D. Goswami, D. H. Trivedi, P. V. Chavan, N. L. Jadhav, D. V. Pinjari, Inorganic Chemistry Communications **181**, 115206 (2025).
[8] D. Nunes, A. Pimentel, R. Branquinho, E. Fortunato, R. Martins, Catalysts **11**, 504 (2021).
[9] X. Jiang, J. Wang, Applied Surface Science **612**, 155849 (2022).
[10] S. J. Babu, M. Muniyappa, B. N. Rao, R. Mudike, M. Shastri, S. Tathagata, P. D. Shivaramu, M. V. Shankar, C. S. A. Kumar, D. Rangappa, International Journal of Hydrogen Energy **47**(95), 40242 (2022).
[11] F. Zabihi, M.-R. Ahmadian-Yazdi, M. Eslamian, Catalysts **7**, 136 (2017).
[12] M. Covei, D. Perniu, C. Bogatu, A. Duta, I. Visa, Surfaces and Interfaces **31**, 102075 (2022).
[13] K. Rustembekkyzy, A. Zholdasbekov, A. Abduvalov, M. Kaikanov, T. S. Atabaev, RSC Advances **13**(49), 34482 (2023).
[14] D. A. S. Mulus, M. D. Permana, Y. Deawati, D. R. Eddy, Applied Surface Science Advances **27**, 100746 (2025).
[15] M. H. Fawey, A. A. A. El-Moula, F. M. El-Hossary, T. Hashem, M. A. El-Kassem, Journal of Materials Science Materials in Electronics **36**(12), 764 (2025).
[16] Z. Bi, D. Deng, Y. Zhang, Y. Xie, Y. Feng, J. Yang, D. Liu, T. Liu, Journal of Alloys and Compounds **1044**, 184484 (2025).
[17] P. R. Dutra, C. C. Amorim, P. L. Gastelois, M. Grao, M. Ratova, A. P. Santos, P. Kelly, Thin Solid Films **792**, 140248 (2024).
[18] N. Xiong, Y. Guo, Y. Nie, Y. Yao, Z. Ying, W. Zhang, R. Liu, X. Wu, H. Zhou, L. Zhou, Y. Wang, J. He, L. Yan, Water **17**, 161 (2025).
[19] H. Yang, X. Zhang, Q. Tao, A. Tanga, J. Optoelectron. Adv. M. **9**(8), 2493 (2007).
[20] T. S. Senthil, N. Muthukumarasamy, S. A. Agilan, M. Thambidurai, K. V. R. Murthy, R. Balasundaraprabhu, J. Optoelectron. Adv. M. **11**(6), 831 (2009).
[21] P. Londhe, N. B. Chaure, A. Athawale, Materials Today Communications **29**, 102924 (2021).
[22] E. S. M. Mouele, S. Ngqoloda, S. Pescetelli, A. Di Carlo, M. Dinu, A. Vladescu, A. C. Parau, A. Agresti, M. Braic, C. J. Arendse, L. F. Petrik, Coatings **10**, 1029 (2020).
[23] N. M. Arifin, E. E. Mhd Noor, F. Mohamad, N. Mohamad, Coatings **14**, 73 (2024).
[24] K. J. A. Yao, B. Hartiti, F. K. Konan, A. Ziti, A. Batan, H. Labrim, A. Laazizi, B. Aka, P. Thevenin, Materials Today: Proceedings, 2024, https://doi.org/10.1016/j.matpr.2024.02.003
[25] N. E. Djehiche, H. Saidi, A. Derbali, A. Attaf, O. B. Khetta, M. S. Aida, R. Bourhefir, R. Toumi, A. Youcef, A. Bouhdjer, Journal of Sol-Gel Science and Technology **117**, 79 (2026).
[26] L. He, D. R. T. Zahn, T. I. Madeira, Materials **16**(15), 5494 (2023).
[27] U. Bellè, D. Spini, B. Del Curto, M. Pedeferri, M. V. Diamanti, Catalysts **13**, 494 (2023).
[28] T. T. D. Nguyen, D. Nguyen, N. N. T. Pham, P. T. Nguyen, Applied Surface Science **683**, 161783 (2024).
[29] L. Wei, X. Xu, L. Zhao, J. Liu, R. Wang, X. Zhang, Optical Materials **154**, 115709 (2024).
[30] W. Chen, T. Qin, Inorganic Chemistry Communications **180**, 115064 (2025).
[31] R. Hatib, K. Anwar, R. Magga, M. A. Astak, D. Widhiyanuriyawan, W. Wardoyo, Journal of Mechanical Engineering Science and Technology (JMEST) **8**(1), 138 (2024).
[32] X. Wang, S. Wang, D. Zhu, X. Huang, J. Optoelectron. Adv. M. **25**(11-12), 594 (2023).
[33] P. B. Nair, V. B. Justinvictor, G. P. Daniel, K. Joy, K. C. James Raju, P. V. Thomas, J. Optoelectron. Adv. M.**16**(3-4), 360 (2014).
[34] L. Andronic, S. Manolache, A. Duta, J. Optoelectron. Adv. M. **9**(5), 1403 (2007).
[35] R. K. Brow, Journal of Non-Crystalline Solids **263-264**, 1 (2000).
[36] A. S. Joshi, E. Elamurugu, S. Leela, Chemical Physics Impact **9**, 100667 (2024).
[37] T. Ivanova, A. Harizanova, T. Koutzarova, B. Vertruyen, Crystals **14**(2), 192 (2024).
[38] K. Yamakawa, Y. Sato, K. Fukutani, The Journal of Chemical Physics **144**(15), 154703 (2016).
[39] A. Prasad, F. Singh, V. Dhuliya, L. Purohit, R. Ramola, Optical Materials **151**, 115411 (2024).
[40] J. Tauc, R. Grigorovici, A. Vancu, Physica Status Solidi B **15**, 627 (1966).
[41] E. Burstein, Physical Review **93**(3), 632 (1954).

*Corresponding author: ana.florea@inoe.ro; ana.iordache@inoe.ro